Statistical Framework for Western North Pacific Tropical Cyclone Landfall Risk through Modulation of the Western Pacific Subtropical High and ENSO

ZACHARY F. JOHNSON,^a DANIEL R. CHAVAS,^a AND HAMISH A. RAMSAY^b

^a Department of Earth, Atmospheric, and Planetary Sciences, Purdue University, West Lafayette, Indiana ^b CSIRO Oceans and Atmosphere, Aspendale, Victoria, Australia

(Manuscript received 22 October 2021, in final form 27 May 2022)

ABSTRACT: Seasonal predictions of tropical cyclone (TC) landfalls are challenging because seasonal landfall count not only depends on the number and spatial distribution of TC genesis, but also whether those TCs are steered toward land or not. Past studies have separately examined genesis and landfall as a function of large-scale ocean and atmospheric environmental conditions. Here, we introduce a practical statistical framework for estimating the seasonal count of TC landfalls as the product of a Poisson model for seasonal TC genesis and a logistic model for landfall probability. We compute spatial variations in TC landfall and genesis by decomposing TC activity in the western North Pacific (WNP) basin into $10^{\circ} \times 10^{\circ}$ bins, then identify coherent regions where El Niño–Southern Oscillation (ENSO) and the western extent of the Pacific subtropical high (WPSH) have significant influences on seasonal landfall count. Our framework shows that ENSO and the WPSH are weakly related to basinwide landfalls but strongly related to regional genesis and landfall probability. ENSO modulates the zonal distribution of TC genesis, consistent with past work, whereas the WPSH modulates the meridional distribution of landfall probability due to variations in steering flow associated with the Pacific subtropical high. These spatial patterns result in four coherent subregions of the WNP basin that define seasonal landfall variations: landfall count increases in the southwestern WNP during a positive WPSH and El Niño, the eastern WNP during a negative WPSH and El Niño, the eastern WNP during a negative WPSH and El Niño, and the northern WNP during a negative WPSH and La Niña.

KEYWORDS: ENSO; Tropical cyclones; Tropical variability

1. Introduction

The East Asia coastline accounts for the most tropical cyclone (TC) landfalls globally, posing a significant risk to life, infrastructure, and local economies. Since the 1970s, landfalling TCs have become ~15% stronger due to climate change, highlighting the importance of accurate seasonal forecasts to assess landfall risk in the coming decades (Mei and Xie 2016; Wang and Toumi 2021). A body of research has advanced seasonal TC forecasts by examining climate factors that impact TC activity in the western North Pacific (WNP) basin, such as spatiotemporal variability in the western Pacific subtropical high and El Niño-Southern Oscillation (ENSO). These climate factors are used to determine seasonal TC activity through statistical and dynamical operational models; however, seasonal landfall forecast skill remains limited because landfall not only depends on the number of TCs but also the probability those TCs are steered toward land:

$$N_{\text{landfall}} = N_{\text{genesis}} \times p_{\text{landfall}}.$$
 (1)

First, variability in TC genesis depends strongly on its thermodynamic environment, and that environment can depend on many climate factors such as ENSO, which describes sea surface temperature (SST) variability in the tropical Pacific (Chan 1985; Lander 1994; Wang and Chan 2002; Camargo and Sobel 2005; Kim et al. 2011; Zhao and Wang 2019). For

Corresponding author: Zachary F. Johnson, zfjohnso@purdue.edu

instance, the warm phase of ENSO, El Niño, causes a south-eastward shift in TC genesis over the WNP basin due to an eastward shift in positive SST anomalies, a decrease in relative humidity near Asia, and the eastward migration of both the lower and upper tropospheric monsoon troughs (Chan 1985; Camargo et al. 2007). This supportive thermodynamic environment allows TCs that form during an El Niño to last longer (Wang and Chan 2002). The opposite is true during ENSO's cold phase, La Niña (C. Wang et al. 2013; Wang and Wu 2016). Although there is a deep understanding of ENSO mechanisms and their influence on TC genesis, predicting ENSO in advance has proved challenging, complicating seasonal TC forecasts.

Second, variability in the westward extension of the North Pacific subtropical high (STH), commonly referred to as the western Pacific subtropical high (WPSH), modulates the large-scale steering flow and hence the TC tracks embedded within that flow (George and Gray 1977; Zhao et al. 2010; Zhao and Wu 2014). During an El Niño, the Pacific STH tends to be weaker, thereby allowing midlatitude troughs to penetrate equatorward, which subsequently favors TCs to recurve on the western periphery of the Pacific STH. During a La Niña, the Pacific STH tends to be stronger, which supports stronger easterlies and favors westward TC tracks (Wang and Chan 2002; Elsner and Liu 2003; Wu et al. 2004; Wu and Wang 2004; Zhang et al. 2012; Zhou and Lu 2019). Other factors contributing to Pacific STH variability include monsoonal heating over land, ocean-atmosphere interactions outside the tropics, and interbasin interactions (Ting 1994; Hoskins 1996; Chen et al. 2001; Wu and Liu 2003; Miyasaka

and Nakamura 2005; Seager et al. 2003; Wang and Wang 2019; Johnson et al. 2020; Sun et al. 2021). B. Wang et al. (2013) describe a region in the western North Pacific (15°-25°N, 115°-150°E) with the highest summertime variance in 850-hPa geopotential height anomalies, which they use to define a WPSH index using an average of the anomalies within this region. Because the WPSH index is highly related to TC movement, Camp et al. (2019) initialized the U.K. Met Office Global Seasonal forecasting system version 5 on 1 May and found significant operational skill predicting the WPSH index during June-August, paving the way to improve seasonal landfall forecasts. Variability in the WPSH is highly predictable due to strong ocean-atmosphere coupling forced by the tropical Pacific, a positive ocean-atmosphere feedback involving the Indo-Pacific warm pool, the tropical Atlantic, and underlying WNP SSTs (Ham et al. 2013; B. Wang et al. 2013; Xiang et al. 2013; Xie et al. 2016).

Seasonal TC landfall forecasts require accurate forecasts of seasonal climate variability such as ENSO and the WPSH and knowledge on how they separately influence regional genesis and landfall probability. Dynamical climate models can simulate large-scale climate variability relevant to TCs (Camp et al. 2015), but a statistical model better represents basinwide TC activity (Choi et al. 2016; Zhang et al. 2017). Yet, skillful seasonal predictions of TC landfalls are challenging because TC genesis, hence landfall probability, responds differently by region despite using the same environmental parameter (Wang and Chan 2002; Lu et al. 2010; Kim et al. 2010; Vecchi and Villarini 2014; Wang et al. 2019). An environmental predictor may also counteract or compound the number of landfalls owing to its separate effect on TC genesis and landfall probability. As past research has focused on genesis and landfall separately using one or more predictors (Yonekura and Hall 2011), to our knowledge, a statistical approach combining a TC genesis and landfall probability model has not been implemented before.

Here, we introduce a statistical framework for assessing seasonal landfall risk related to the WPSH and ENSO. Our principal research questions are:

- Can we develop a simple model framework for TC landfalls that accounts for both genesis and landfall probability?
- 2) How do TC landfall probability and genesis in the WNP basin vary spatially with respect to ENSO and WPSH variability?
- 3) Are the results from the statistical framework consistent with observed tracks in high and low landfall seasons?

To answer these questions, we first statistically model seasonal landfalls by the product of a Poisson regression for seasonal TC genesis and logistic regression for the probability of landfall for each storm. Next, we decompose the spatial distributions of each across the entire WNP basin to identify coherent regions where ENSO and the WPSH significantly influence TC genesis and landfall probability. Last, we spatially aggregate these coherent regions and examine how genesis, landfall probability, and landfall count from each region

vary with seasonal ENSO and WPSH indices. We detail the model framework in section 2. Then we describe our results using the statistical framework in section 3, followed by a discussion with concluding remarks in section 4.

2. Data and methods

a. Tropical cyclone data

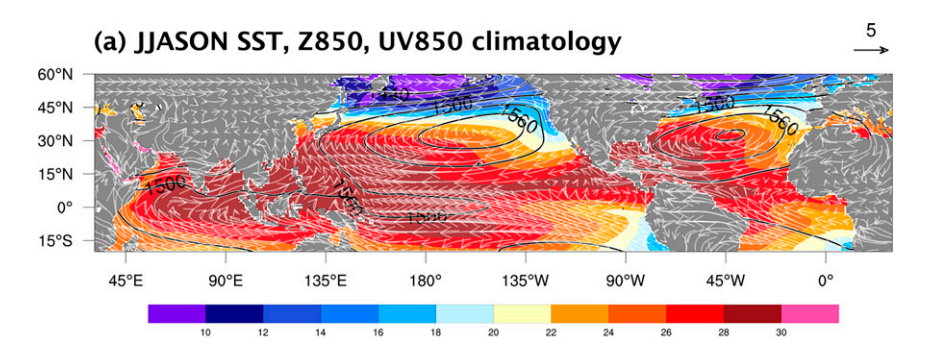
TC data in the WNP basin are obtained from the International Best Track Archive for Climate Stewardship, version 4 (IBTrACSv4) (Knapp et al. 2010). WNP basin TCs are extracted from the Joint Typhoon Warming Center (JTWC) in the IBTrACSv4 dataset from 1979 to 2020 during the June-November (JJASON) season. We define two variables to quantify TC genesis count and landfall probability, respectively: N_{genesis} and p_{landfall} . Genesis is defined when a TC first achieves tropical depression status, and dissipation is defined when a TC last falls below tropical depression status. This study only counts TCs that achieve tropical storm status ($>17.5 \text{ m s}^{-1}$). Landfall is determined by the time and location a cyclone strikes a landmass greater than 1400 km² within 6 h of the observation in IBTrACS similar to other studies (e.g., Yang and Chen 2021; Wang and Toumi 2022). Example landmasses greater than 1400 km² in the western North Pacific include Taiwan (~32 260 km²), Jeju Island (~1826 km²), most of the Philippines, but not the Babuyan Islands (<200 km²) nor the surrounding islands near Okinawa (<1207 km²). A landfall may occur in December if genesis is achieved in the JJASON season. Long-term trends of TC genesis and landfall are not removed in the following analysis.

b. Reanalysis data

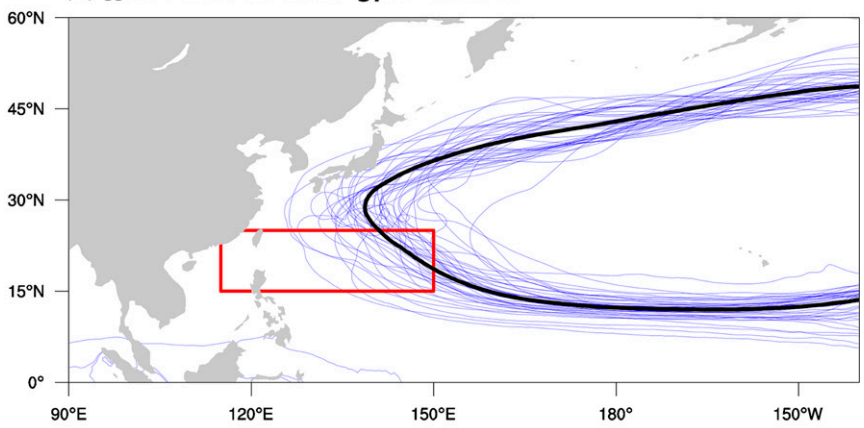
To assess the WPSH, we obtain European Centre for Medium-Range Weather Forecasts (ECMWF) reanalysis ERA5 monthly 850-hPa geopotential height (Z850) (Hersbach 2016), calculate anomalies based on the 1979–2020 mean, and produce an area average over the western North Pacific (15°–25°N, 115°–150°E), previously defined by B. Wang et al. (2013). Additionally, we use the Centennial in situ Observation-Based Estimate SST (COBE-SST) (Ishii et al. 2005), calculate anomalies based on the 1979–2020 mean, and obtain the monthly Niño-3.4 index (5°–5°N, 170°–120°W). We limit ERA5 and COBE-SST datasets to the June–November season (JJASON) for the following analyses. The linear trends at each grid point are extracted from the anomalies to remove the long-term trend, such as the global warming component.

c. Statistical framework

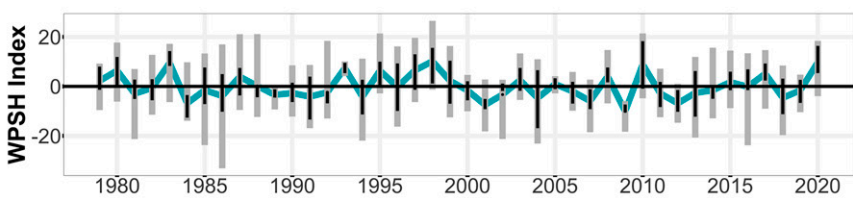
Landfall requires two components: (i) TC genesis and (ii) the steering of the TC into the coastline. To keep our framework as simple as possible, we consider landfall anywhere along the East Asia coastline. Each TC is assigned a 1 if it makes landfall anywhere along the coastline or 0 if it does not. Once formed, a given TC thus has some probability of making landfall. Hence, we model landfall count (N_{landfall}) by considering the temporal variability in both seasonal TC genesis count (N_{genesis}) and the probability



(b) JJASON Z850 1510 gpm contour



(c) WPSH index



(d) Niño3.4 index

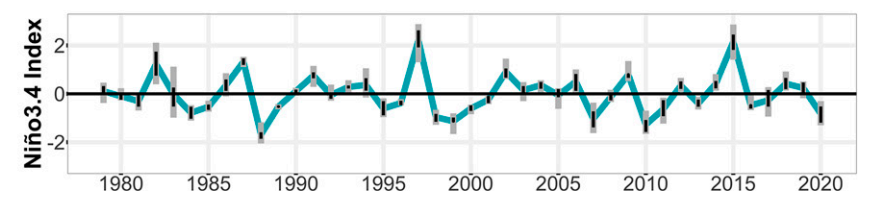


FIG. 1. The Pacific subtropical high depicted as (a) the 1979–2020 climatology of JJASON 850-hPa geopotential height in geopotential meters (m; contours), 850-hPa UV winds (m s⁻¹; arrows), and SST (°C; colors). The reference vector is located at the top-right of the plot. Z850 contour intervals are 30 m. (b) JJASON Z850 1510-m contours (blue contours) for each season (1979–2020) and the climatological JJASON Z850 1510-m contour (black). (c) The JJASON WPSH index and (d) JJASON Niño-3.4 index (light blue) with vertical bars representing monthly variability of the WPSH and Niño-3.4 indices from maximum to minimum (gray bars) and interquartile range (25th–75th percentile; black bars). The red box represents the area averaged to produce the WPSH index (15°–25°N, 115°–150°E) from B. Wang et al. (2013) and Camp et al. (2019). The Niño-3.4 index is computed by monthly detrended SST anomalies averaged over 5°S–5°N, 170°–120°W.

100°W

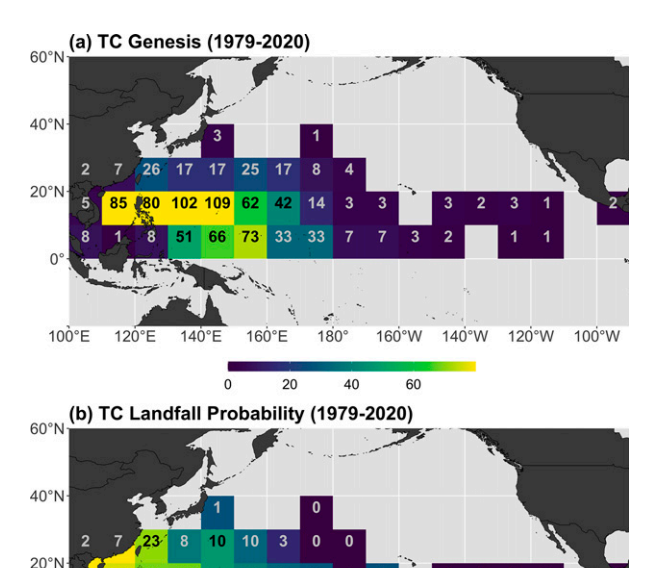


FIG. 2. Climatological TC (a) genesis and (b) landfall probability split into $10^{\circ} \times 10^{\circ}$ bins (colors) from 1979 to 2020. For each given bin, the number refers to the (a) TC genesis count and (b) TC landfall count. Note that some numbers are overlaid on land despite the tile having a portion over water.

20%

each individual storm to make landfall ($p_{\rm landfall}$) as shown in Eq. (1). The seasonal number of basinwide landfalls ($N_{\rm landfall}$) is the product of a Poisson regression for seasonal TC genesis ($N_{\rm genesis}$) and a logistic regression modeling landfall probability ($p_{\rm landfall}$).

d. Statistical models

We model seasonal genesis using a Poisson regression (i.e., log-link linear), as has been done in past work for modeling counts (Yonekura and Hall 2011), which are positive-definite (Elsner and Schmertmann 1993). We include two covariates: the seasonal JJASON Niño-3.4 and WPSH indices:

$$\ln(N_{\text{genesis}}) = \beta_{\text{Nifio3.4}_{\text{enl}}} X_{\text{Nifio3.4}_{\text{enl}}} + \beta_{\text{WPSH}_{\text{enl}}} X_{\text{WPSH}_{\text{enl}}} + \beta_0, \tag{2}$$

$$N_{\text{genesis}} = \exp(\beta_{\text{Niño3.4}_{\text{snl}}} X_{\text{Niño3.4}_{\text{snl}}} + \beta_{\text{WPSH}_{\text{snl}}} X_{\text{WPSH}_{\text{snl}}} + \beta_0), \tag{3}$$

where $N_{\rm genesis}$ is the seasonal genesis count, $X_{\rm Niño3.4}$ is the Niño-3.4 index, $X_{\rm WPSH}$ is the WPSH index, $\beta_{\rm Niño3.4}$ and $\beta_{\rm WPSH}$ are the regression coefficients for each, and β_0 is the intercept. The subscript "snl" indicates the seasonal JJASON average.

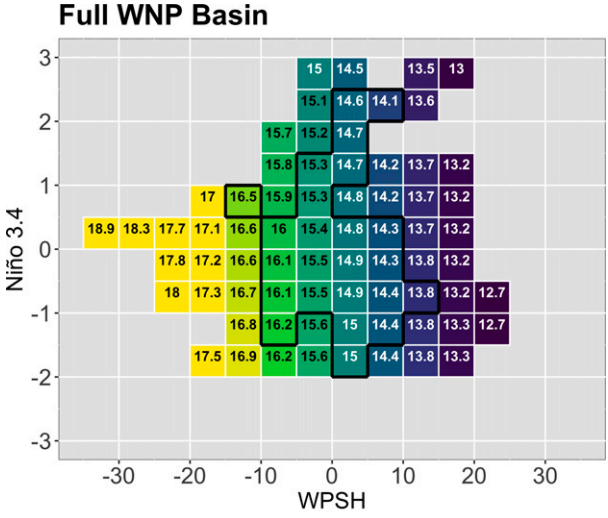


FIG. 3. Heat map of modeled seasonal landfall count for the entire WNP basin from our statistical framework [Eq. (1)] with seasonal Niño-3.4 and the WPSH as covariates. Extent of tiles indicates Niño-3.4 and WPSH indices falling within observed monthly values with the seasonal averages of those values within the black outlined polygon.

15

16

17

14

For landfall probability, where landfall is either 1 or 0 for yes or no, respectively, the preferred choice for regression is logistic regression (Saunders et al. 2000; Christensen 2006). We model landfall probability using a logistic regression with Niño-3.4 and WPSH indices for each storm as covariates to describe the log-odds:

$$\ln\left(\frac{p_{\text{landfall}}}{p_{\text{landfall}}-1}\right) = \beta_{\text{Niño3.4}_{\text{mon}}} X_{\text{Niño3.4}_{\text{mon}}} + \beta_{\text{WPSH}_{\text{mon}}} X_{\text{WPSH}_{\text{mon}}} + \beta_{0}, \tag{4}$$

$$p_{\text{landfall}} = \frac{\exp(\beta_{\text{Niño3.4}_{\text{mon}}} X_{\text{Niño3.4}_{\text{mon}}} + \beta_{\text{WPSH}_{\text{mon}}} X_{\text{WPSH}_{\text{mon}}} + \beta_0)}{1 + \exp(\beta_{\text{Niño3.4}_{\text{mon}}} X_{\text{Niño3.4}_{\text{mon}}} + \beta_{\text{WPSH}_{\text{mon}}} X_{\text{WPSH}_{\text{mon}}} + \beta_0)}, \tag{5}$$

where p_{landfall} is probability of landfall for each storm, $X_{\text{Niño3.4}}$ is the Niño-3.4 index, X_{WPSH} is the WPSH index, $\beta_{\text{Niño3.4}}$ and β_{WPSH} are the regression coefficients for each, and β_{0} is the intercept. In the logistic model, each TC has an associated WPSH and Niño-3.4 index. We linearly interpolate monthly WPSH and Niño-3.4 indices into daily values and compute an index for each TC track as described by the subscript "mon" for monthly interpolated values. For instance, if a TC track from genesis to dissipation lasts 15 days from 25 June to 9 July, we will assign the daily linearly interpolated indices from those 15 days and average them to produce a single observation for the TC track. By linearly interpolating monthly indices into daily indices, we remove higher frequency synoptic variability, thereby focusing on the low-frequency

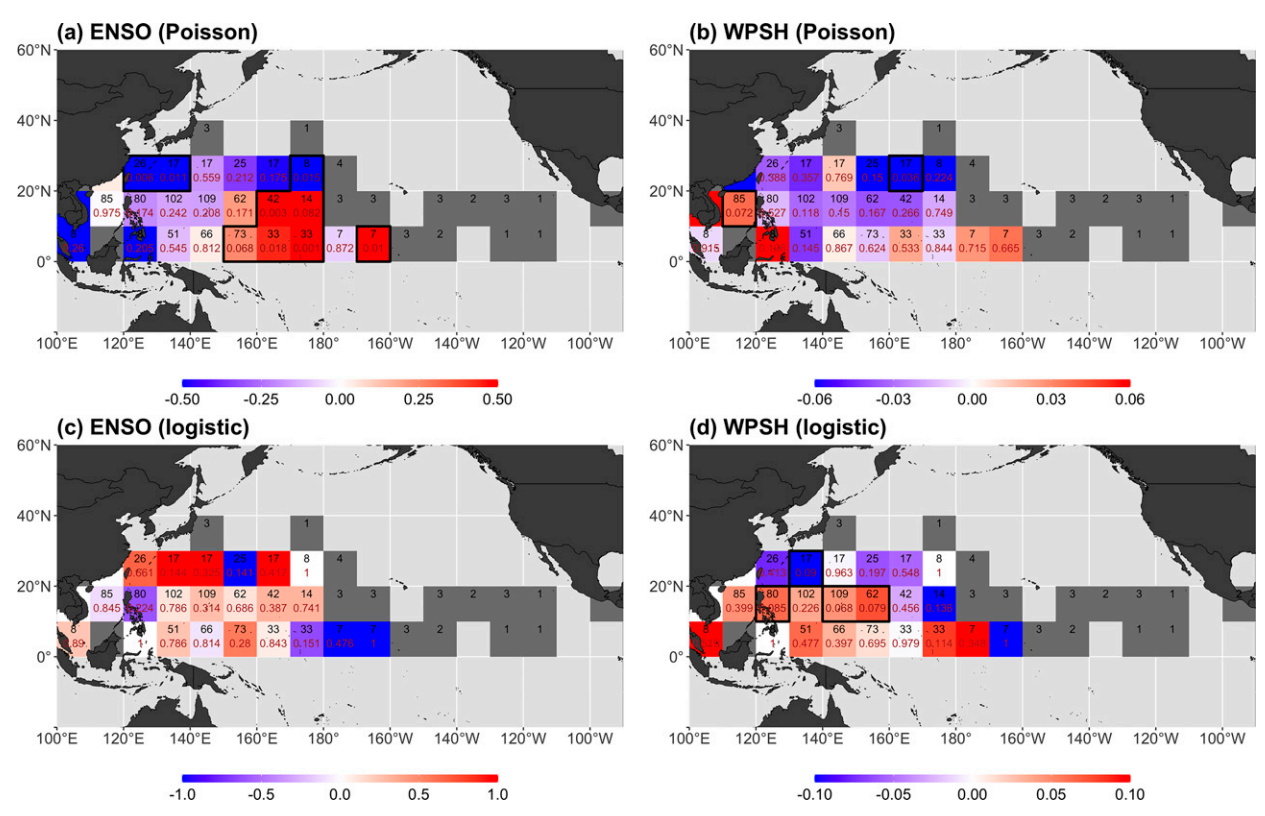


FIG. 4. Regression maps of (top) TC genesis and (bottom) TC landfall following the Poisson regression and logistic regression models where (colors) depict regression coefficients, β_{WPSH} and $\beta_{\text{Niño3.4}}$, corresponding to (a),(c) Niño-3.4 and (b),(d) WPSH indices, respectively, within $10^{\circ} \times 10^{\circ}$ bins. The top number in each bin represents TC count, and the bottom number represents the associated p value corresponding to the regression coefficients. The p values smaller than 0.1 (90% statistical significance level) are outlined in black. Regression coefficients are only shown if more than 7 TCs form or otherwise are grayed out.

components of the WPSH and ENSO that is more relevant to seasonal forecasting.

e. Model application

Using the model framework, we first apply the Poisson and logistic regression for the entire WNP basin to describe the dependencies of seasonal WPSH and ENSO on seasonal basinwide landfall count. Our framework can also be applied to any subset of TCs. In our case, we subset spatially:

$$N_{\text{landfall}}^{i} = N_{\text{genesis}}^{i} \times p_{\text{landfall}}^{i}, \tag{6}$$

where i refers to the region i out of N regions (for the entire basin N=1). We next apply the Poisson and logistic regressions within $10^{\circ} \times 10^{\circ}$ bins to describe the spatial dependencies of ENSO and the WPSH on seasonal genesis count and landfall probability within the WNP basin. By doing so, we expect the sample size to be too small to define significant signals for any given bin, but it provides an opportunity to identify coherent regions where ENSO and the WPSH have significant influences on TC genesis and landfall probability. We can then aggregate the like-signed coherent regions to increase sample sizes and thus achieve statistical significance as well as allow for a simpler interpretation of the spatial

variability. We visualize observed genesis and TC tracks for high and low landfall season in each region based on the model's estimate. Finally, we use the model's estimate to identify high and low landfall seasons to characterize the observed track differences.

3. Results

a. Climatology of the North Pacific STH

Before describing the results of the statistical framework, we begin simply by depicting the climatological state of the summer–fall Pacific basin. The climatological steering flow over the WNP basin is dominated by the WPSH, as depicted in Fig. 1a. A broad area of atmospheric high pressure emerges over summer and fall (June–November), encompassing most of the North Pacific with its center over the eastern two-thirds of the basin at about 35°N. A similar feature also emerges over the North Atlantic Ocean (Seager et al. 2003). This zonally elongated North Pacific high pressure extends toward the tropics, providing easterly trade winds and promoting warm water in the WNP basin. Over the WNP basin, the climatological easterlies turn to southeasterly winds, allowing a meridional component to the steering flow at the western periphery of the Pacific STH. The steering flow over the WNP basin has

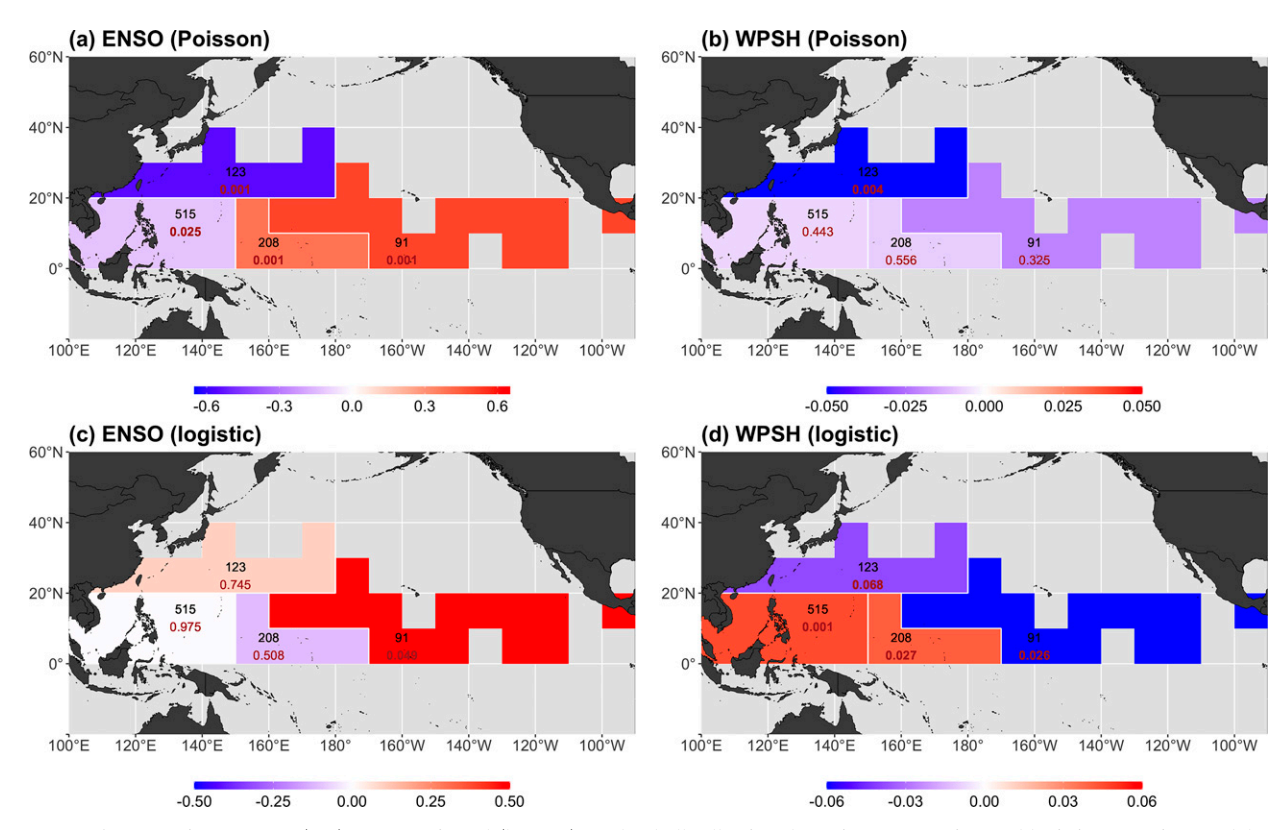


FIG. 5. Regression maps of (top) TC genesis and (bottom) TC landfall following the Poisson regression and logistic regression models, where (colors) depict regression coefficients corresponding to (a),(c) Ni \bar{n} o-3.4 and (b),(d) WPSH indices, respectively, for each coherent region identified in Fig. 4. The top number in each bin represents TC count, and the bottom number depicts the associated p value corresponding to the regression coefficient for the given region. The p values smaller than 0.1 (90% statistical significance level) are in bold.

significant variability due to changes in the WPSH (Camp et al. 2015).

b. Variability in the WPSH and ENSO

To identify the mechanism responsible for steering TCs into land or out to sea, we show the variability in the mean June–November westward extent of the Pacific STH in Fig. 1b. The summer and fall average 1510-m Z850 contour exhibits significant seasonal variability. Some seasons show the 1510-m Z850 contour extending near the Asia coastline, while other seasons depict it in the west-central subtropical North Pacific, corresponding to a stronger and weaker Pacific STH, respectively. To quantify the aforementioned variability, Camp et al. (2015) produced the western Pacific subtropical high (WPSH) index shown in Fig. 1c. Seasonal variability in the WPSH exhibits interannual-to-decadal variability (blue line in Fig. 1c), suggesting season-to-season changes in the steering flow for TCs (Elsner and Liu 2003; Wu et al. 2004).

Although low-frequency variability in the WPSH exists, we also see intraseasonal variability as shown in Fig. 1c (vertical bars). Generally, most seasons feature a month with both a negative and positive WPSH index, but exceptions exist (e.g., 1993 and 2009). Some seasons (e.g., 1986, 1994, and 2004) feature significant intraseasonal variability, while others have minimal intraseasonal variability (e.g., 1989, 1993, and 2005).

These intraseasonal variations in the WPSH have the potential to cause changes in TC genesis and/or landfall through changes in the steering flow pattern (Chen et al. 2009, 2019, 2020).

In contrast with the WPSH, the summer–fall Niño-3.4 index varies slowly at intraseasonal time scales (Fig. 1d). June–November seasonal Niño-3.4 and WPSH indices are weakly correlated (R = -0.10), and the monthly values are also weakly correlated except for November (R = 0.02, -0.07, -0.25, -0.02, 0.10, and 0.60 for June, July, August, September, October, and November, respectively). Our statistical framework treats the Niño-3.4 and WPSH indices as independent factors due to the weak monthly and seasonal correlations.

c. Basinwide TC analysis

Figure 2 shows climatological maps of TC genesis and land-fall probability from 1979 to 2020 in the June–November TC season, depicting regional differences between increased genesis and landfall probability. Notably, more TCs form in the 10°N–20°N band, West of 150°E (Fig. 2a). In contrast, landfall probability increases toward the South and West and decreases toward the east and north (Fig. 2b). In other words, TCs that form near the Philippines, China, or the Vietnam coasts have a high climatological likelihood of making landfall (>80%). In contrast, TCs that form in the central Tropical

TABLE 1. Table of regression coefficients and p values for regions defined in Fig. 5. The N_{storm} and P_{landfall} columns show regression coefficients for the WPSH and Niño 3.4 indices in each cell. All intercepts are statistically significant (>99.9%).

Region	Variable	N _{storm} (Poisson)	P _{value} (Poisson)	P _{landfall} (logistic)	P _{value} (logistic)	Important terms
Southwest	WPSH	-0.0067	0.4433	0.0456	0.0005	Poisson: Niño-3.4
	Niño-3.4	-0.1274	0.025	-0.005	0.9747	Logistic: WPSH
South-central	WPSH	-0.0083	0.5560	0.0413	0.0269	Poisson: Niño-3.4
	Niño-3.4	0.3885	< 0.001	-0.112	0.5079	Logistic: WPSH
East	WPSH	-0.0214	0.3253	-0.0637	0.0261	Poisson: Niño-3.4
	Niño-3.4	0.5067	1.47×10^{-5}	0.5244	0.0494	Logistic: Niño-3.4, WPSH
North	WPSH	-0.0537	0.0045	-0.0386	0.0683	Poisson: Niño-3.4, WPSH
	Niño-3.4	-0.5489	< 0.001	0.0965	0.7455	Logistic: WPSH

Pacific have a lower likelihood of making landfall (~40%). Meanwhile, landfall probability and TC genesis are both high in the South China Sea and the Philippines Sea.

Using the Poisson and logistic regression approach outlined in the section 2, we find the only statistically significant predictor (i.e., p < 0.1) is the seasonal WPSH index for genesis, while Niño-3.4 for genesis, and Niño-3.4 and WPSH for landfall probability are insignificant ($p \ge 0.1$). We produce a heat map describing the range of seasonal basinwide landfalls based on the seasonal Niño-3.4 and the WPSH indices in Fig. 3. Basinwide, TC landfall dependencies on Niño-3.4 and the WPSH only depict a range from 14 to 16 (within black box depicting seasonal observations), with a weak dependence on the WPSH index and no dependence on Niño-3.4. Figure 3 shows increased landfalls during a weak WPSH and a La Niña pattern. These results imply that we must spatially decompose TC genesis and landfall in the WNP basin to identify coherent regions where the WPSH and ENSO influence seasonal landfall count.

d. Spatial variability in TC genesis and landfall probability

We next examine the spatial variability in the dependence of genesis and landfall probability on the WPSH and ENSO (Fig. 4). For genesis, Fig. 4a shows TC genesis regressed on the Niño-3.4 index, depicting a coherent ENSO pattern with a positive relationship in the eastern half of the WNP basin south of 20°N and a negative one in the western half of the

WNP basin. An El Niño pattern promotes a supportive thermodynamic environment for TCs south of 20°N and east of 150°E, and an inhibiting environment west of 150°E and north of 20°N. Also in Fig. 4a, many tiles contain statistically significant p values, mainly for the positive regression coefficients toward the east (bold brown numbers in Fig. 4a). In contrast with ENSO, Fig. 4b shows the WPSH having a noisy pattern, with a general negative relationship with TC genesis, but nearly all tiles are statistically insignificant. An exception of a $10^{\circ} \times 10^{\circ}$ tile centered at 15°N, 115°E over the South China sea shows a p value of 0.07, suggesting TC genesis may depend on the WPSH there (B. Wang et al. 2013). As a result, June-November TC genesis is primarily driven by ENSO, with the WPSH playing a lesser role. These results are consistent with past research describing how ENSO modulates the zonal distribution of TC genesis (Gray 1979; Chan 1985; Gray and Sheaffer 1991; Camargo et al. 2007).

For landfall probability (Figs. 4c,d), ENSO depicts an inconsistent relationship with no tiles achieving statistical significance, but the WPSH is characterized by a dipolar north–south pattern for landfall probability. Figure 4d shows a positive relationship south of 20°N and extending from the Southeast Asia coastline into the central tropical Pacific, whereas we see a negative relationship in the 20°–30°N band. These results suggest that when cyclones form closer to the equator, they will be steered into (away from) land during a strong (weak) WPSH. Meanwhile, toward the north, the

TABLE 2. Table of Poisson and logistic regression equations for regions defined in Fig. 5 for only statistically significant variables in Table 1 (right column). All predictors exceed the 95% statistical significance level. We also show the climatological storm count, landfall probability, and number of landfalls for each region in columns N_{storm} , P_{landfall} , and N_{landfall} , respectively.

Region	Equation	$N_{\rm storm}$ (storms yr ⁻¹)	$P_{ m landfall}$	N_{landfall} (landfalls yr ⁻¹)
Southwest	$\ln(N_{\text{genesis}}) = -0.1213X_{\text{Niño}3.4} + 2.5017$	12.26	0.82	10.09
	$\ln\left(\frac{p_{\text{landfall}}}{p_{\text{landfall}} - 1}\right) = 0.045 65 X_{\text{WPSH}} + 1.6665$			
South-central	$\ln(N_{\text{genesis}}) = -0.3860 X_{\text{Niño}3.4} + 1.5471$	4.95	0.58	2.86
	$\ln\left(\frac{P_{\text{landfall}}}{p_{\text{landfall}}-1}\right) = 0.0378X_{\text{WPSH}} + 0.3257$			
East	$\ln(N_{\text{genesis}}) = -0.4935 X_{\text{Niño}3.4} + 0.6851$	2.17	0.29	0.62
	$\ln\left(\frac{p_{\text{landfall}}}{p_{\text{landfall}} - 1}\right) = 0.5244X_{\text{Niño3.4}} - 0.0637X_{\text{WPSH}} - 1.3033$			
North	$\ln(N_{\text{genesis}}) = -0.5489 X_{\text{Niño}3.4} - 0.0537 X_{\text{WPSH}} + 0.9644$	2.93	0.52	1.52
	$\ln\left(\frac{p_{\text{landfall}}}{p_{\text{landfall}} - 1}\right) = -0.0407X_{\text{WPSH}} + 0.0249$			

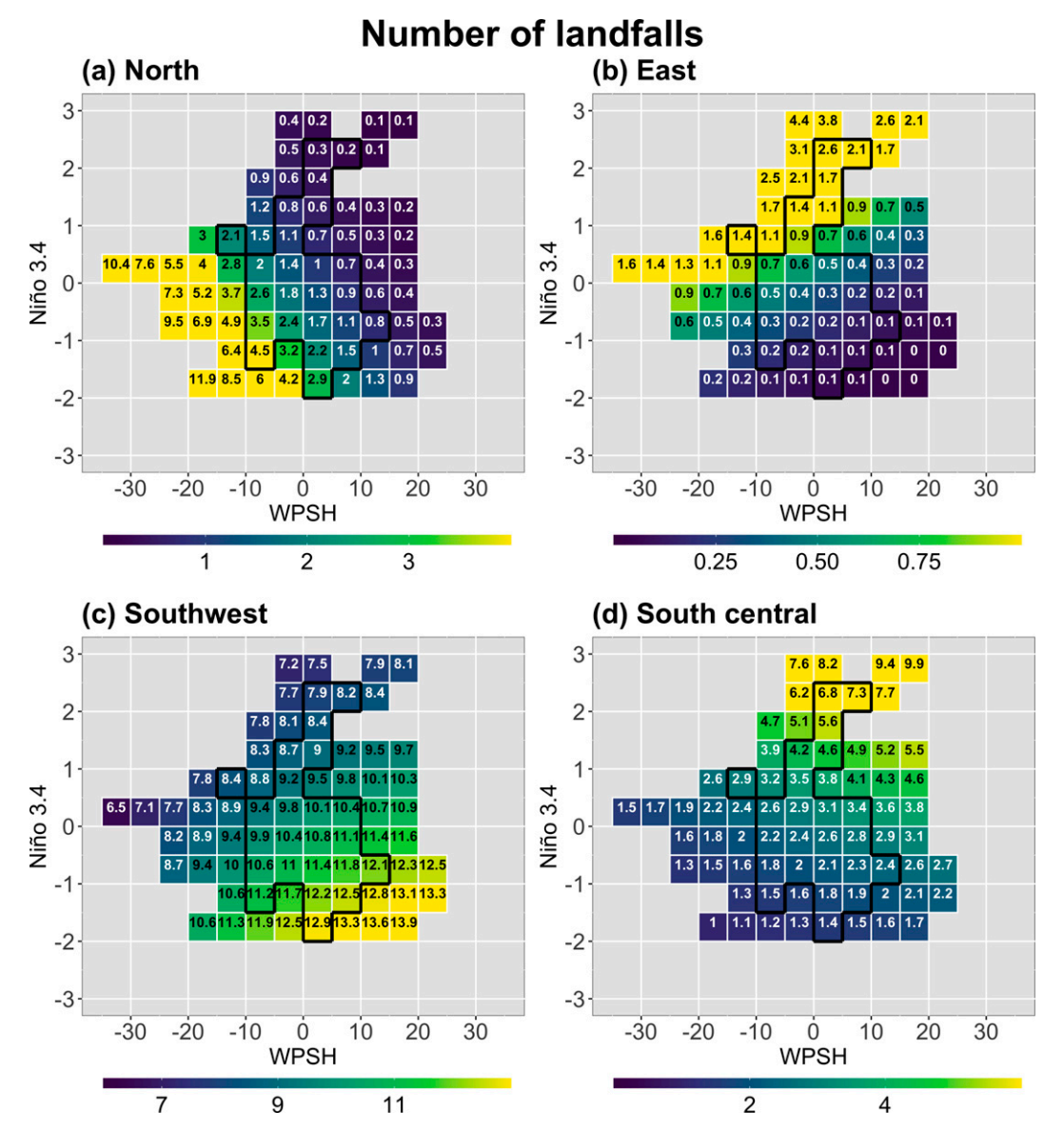


FIG. 6. Heat map of modeled seasonal landfall count for each given region defined in Fig. 5 from our statistical framework [Eq. (1)] with seasonal Niño-3.4 and the WPSH as covariates. Extent of tiles indicates Niño-3.4 and WPSH indices falling within observed monthly values with the seasonal averages of those values within the black outlined polygon.

negative relationship suggests when TCs form there, they will be steered out to sea (into land) during a strong (weak) WPSH. A strong WPSH corresponds to enhanced easterlies toward the south, enhanced northerlies at the western periphery of the STH, and enhanced westerlies toward the north (B. Wang et al. 2013). The opposite is true for a weaker WPSH. These results complement Fig. 1a, showing climatological steering flow having a more easterly component toward the south and a westerly component to the north.

Based on the zonal contrast of TC genesis when regressed on the Niño-3.4 index (Fig. 4a) and the meridional contrast of TC landfall when regressed on the WPSH index (Fig. 4d), we may define four coherent regions for TC genesis and

landfall probability dependencies on ENSO and the WPSH (Fig. 5 and Table 1). Statistical significance is achieved in all regions when we regress TC genesis upon the Niño-3.4 index (Fig. 5a), and only the north region when TC genesis is regressed upon the WPSH index (Fig. 5b). For TC landfall probability, statistical significance is achieved in all regions when we regress TC landfall on the WPSH index (Fig. 5d), and only the east region in the central tropical Pacific when TC landfall is regressed on the Niño-3.4 index (Fig. 5c). These results imply that these four regions have distinct dependencies of ENSO and the WPSH on seasonal landfall count.

In the southwest region in Fig. 5, which accounts for 55% of all TCs, we find that the Niño-3.4 index is statistically

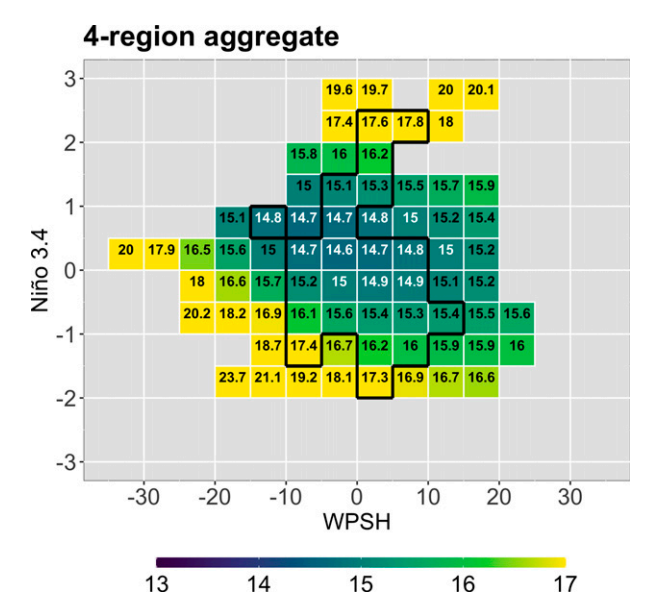


FIG. 7. Modeled seasonal basinwide landfall count calculated by summing modeled landfall counts from all four regions based on Fig. 6. Extent of tiles indicate Niño-3.4 and WPSH indices falling within observed monthly values with the seasonal averages of those values within the black outlined polygon.

significant for TC genesis and WPSH index for TC landfall (Table 1). Similarly, we find the same variables to be statistically significant for the south-central region. These two regions account for 77% of all TCs, yet they have opposing Niño-3.4 coefficients due to the close inverse relationship between the SST anomalies in the western Pacific warm pool and those in the Niño-3.4 region (Yonekura and Hall 2011; Capotondi et al. 2015). The western extent of the positive SST anomalies during an El Niño correspond to a north-south boundary at 150°W, describing the opposite phase coefficients between the southeast and south-central regions in Figs. 4a and 5a (Williams and Patricola 2018). In the east region, which accounts for only 10% of all TCs, the Niño-3.4 index is a statistically significant predictor for TC genesis and both Niño-3.4 and the WPSH indices are statistically significant for TC landfall. Last, the north region shows both Niño-3.4 and the WPSH indices as statistically significant terms for TC genesis, but only the WPSH for TC landfall. In the following analysis, we remove the statistically insignificant predictors, rerun the statistical models, and show updated regression equations in Table 2. None of the regression coefficients change phase, with only minor changes in the coefficient's amplitude from Table 1.

To examine the range of landfall possibilities, we produce heat maps of estimated landfall count for storms that form within each region in Fig. 6 using the equations in Table 2 to highlight the range of modeled seasonal landfall counts for a given seasonal WPSH and Niño-3.4 index. In the southwest region, the number of landfalls is increased from ~8 to ~13 during a strong La Niña and a strong WPSH compared to a strong El Niño and weak WPSH (Fig. 5d). This result indicates that

La Niña conditions (positive SST anomalies in southwest WNP) fosters increased TC genesis, and subsequently, during a strong WPSH, those TCs are more likely to be steered into land (Table 2).

For the south-central region (Fig. 6d), an El Niño and a strong WPSH increases the number of landfalls from ~1 to ~7 compared to a La Niña and weak WPSH. For the eastern region encompassing the central and North Pacific (Fig. 6b), an El Niño favors an increase from 0 to ~3 landfalls due to the compounding effect of ENSO on genesis and landfall probability (third row in Table 2). Last, the north region shows a significant increase in landfalls during a weak WPSH with a lesser effect of ENSO. This significant increase in landfalls in the northern region during a weak WPSH is related to the compounding effect of a negative WPSH index on genesis and landfall probability (last row in Table 2) with a possible range from 0 to ~5 landfalls. While we find a dependence of seasonal ENSO and the WPSH on seasonal landfalls in these four regions, when we add them together to estimate total basinwide landfall count in Fig. 7, we find a weak dependence, similar to when we apply the statistical model to the basinwide seasonal genesis and landfalls in Fig. 3. We see a more complex structure to the dependence in Fig. 7 than found in Fig. 3 because the increased degrees of freedom that comes from modeling the four regions separately. This result further supports a weak dependence of seasonal ENSO and the WPSH on basinwide landfalls. Instead, Fig. 6 supports strong, offsetting regional variations on the dependence of ENSO and the WPSH on seasonal landfalls.

e. Tracks in high versus low predicted landfall seasons

Last, Figs. 8 and 9 depict observed composite plots of TC genesis points and their associated tracks for each region based on seasons with high and low landfall counts from our statistical framework (bright and dark colors in Fig. 6, respectively). In the southwest region, the landfall probability ranges from ~89% to ~74% for high and low landfall composites, respectively (Figs. 8c and 9c). The lower landfall probability for low composites is due to more tracks recurving away from the Asia coastline, in agreement with a negative mean −5.8 WPSH index associated with TC tracks in those composite seasons (Fig. 9c). In contrast, Fig. 8c shows more straight-lined tracks for high composite seasons associated with a strong +7.9 WPSH index. Meanwhile, the south-central region shows a greater landfall probability difference: ~59% compared to ~17% for high and low landfall composites, respectively (Figs. 8d and 9d). Likewise, we see significantly more straight-lined TC tracks for high composite seasons compared to more recurving TC tracks in low composite seasons, agreeing with negative -7.4 and positive +6.1 WPSH indices, respectively.

For the east and north regions, more cyclones form and make landfall for high landfall composite seasons in contrast to low landfall composite seasons (Figs. 8a,b and 9a,b). For low composite seasons, only a few storms form in east and north regions. In the east region for high composite seasons, many cyclones track toward the Japan coast associated with a WPSH of -1.16, but a Niño-3.4 index of +1.55 (Fig. 8b). This result is consistent with the compounding positive effect of ENSO for

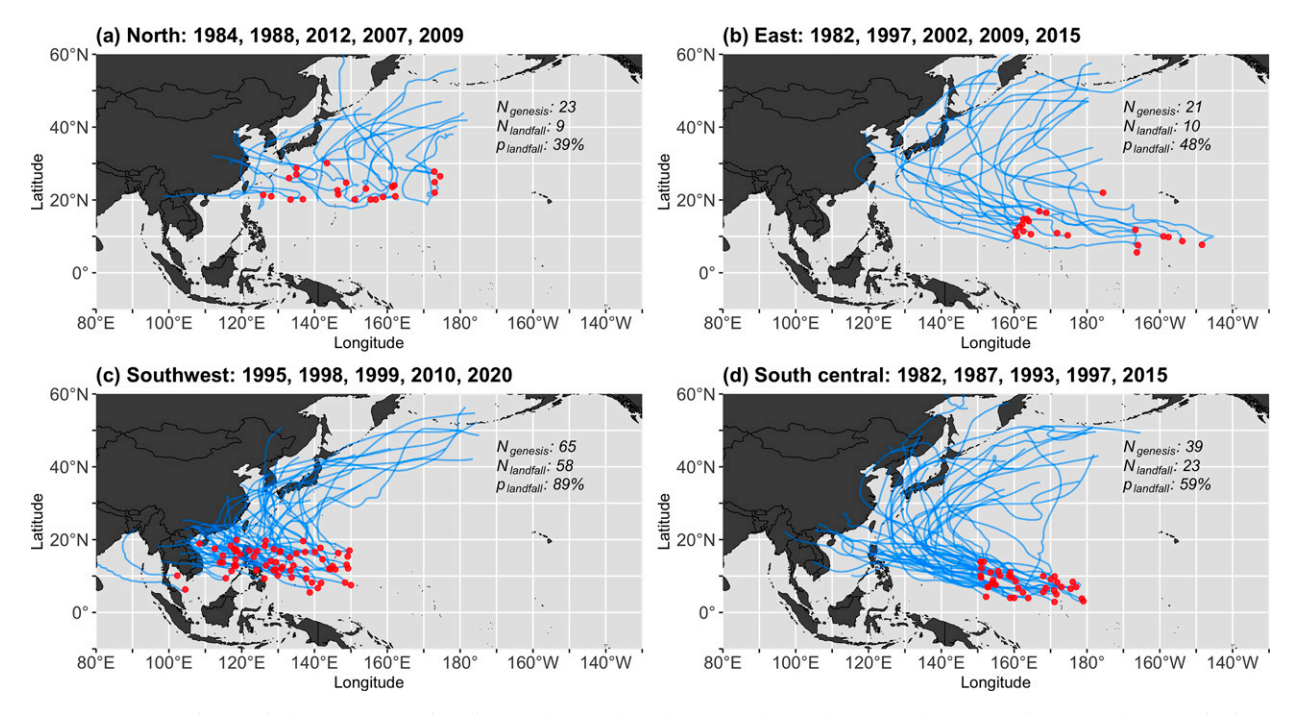


FIG. 8. Composite tropical cyclone genesis points and tracks based on five observed seasons that have Niño-3.4 and WPSH indices located in high modeled landfall count (bright colors) on Fig. 6 for each region. The terms N_{genesis} , N_{landfall} , and p_{landfall} describe the number of cyclones, the number of those cyclones that made landfall, and the composite seasonal landfall probability, respectively.

both genesis and landfall probability in the east region (Table 2). For the north region in Fig. 8a, the high composite shows TC tracks making landfall in northern China, the Korean Peninsula, and Japan, but the WPSH is near its climatological mean (-0.85). However, the Niño-3.4 is -0.58, a significant predictor for TC genesis in the north region (Table 2). Based on the significant regression coefficients in our framework and the high landfall composites in the north, TC genesis may be the dominant component for seasonal landfalls there.

Although not explicitly modeled, a relationship exists between seasonal TC genesis and seasonal TC landfall probability in the east region (R=0.5), whereas weak relationships exist in the other regions (R=-0.04, 0.11, and -0.07 in the southwest, south-central, and north regions). As a result, when more storms form in the east region, we have increased landfall probability, along with the effects of the WPSH and ENSO. Overall, the observed composites based on the modeled seasonal landfall counts help to visualize the dependencies identified by our statistical framework for estimating regional variation in high and low landfall seasons in the WNP basin.

4. Discussion and conclusions

TC landfall depends on both the genesis of a TC and the probability that the TC will make landfall. This work developed a simple statistical framework to estimate seasonal landfall count dependencies on ENSO and the WPSH using the product of a Poisson model for genesis and a logistic model for landfall probability. Our Poisson genesis model demonstrates that ENSO modulates the zonal distribution of summer–fall TC genesis,

consistent with previous studies (Gray 1979; Chan 1985; Dong 1988; Wu and Lau 1992; Lander 1994; Chia and Ropelewski 2002; Clark and Chu 2002; Zhao et al. 2010). Meanwhile, the logistic landfall probability model demonstrates that the WPSH modulates the meridional distribution of landfall probability due to variations of the western periphery of the Pacific subtropical high. The key findings of this study are as follows:

- 1) Basinwide seasonal landfall count shows a weak dependence on ENSO and the WPSH.
- Four coherent regions in the WNP basin characterize the dependence of ENSO and the WPSH on the seasonal number of landfalls.
- 3) An El Niño enhances TC genesis in the eastern WNP basin and inhibits TC genesis in the western WNP basin, whereas a strong WPSH increases landfall probability in the southern WNP basin and decreases landfall probability in the northern WNP basin.
- 4) Accounting for ~55% of total WNP cyclones, the south-west WNP basin has the greatest seasonal number of TC landfalls, but the south-central, eastern, and northern regions in the WNP basin show a wide range of seasonal TC landfalls depending on ENSO and the WPSH.
- 5) Our statistical framework shows high landfall seasons are characterized by increased straight-lined tracks associated with a stronger WPSH, whereas low landfall seasons are characterized by recurving tracks out to sea in the northern Pacific associated with a weaker WPSH.

In the southwest region, seasonal landfall count increases during La Niña and a strong WPSH. In the south-central

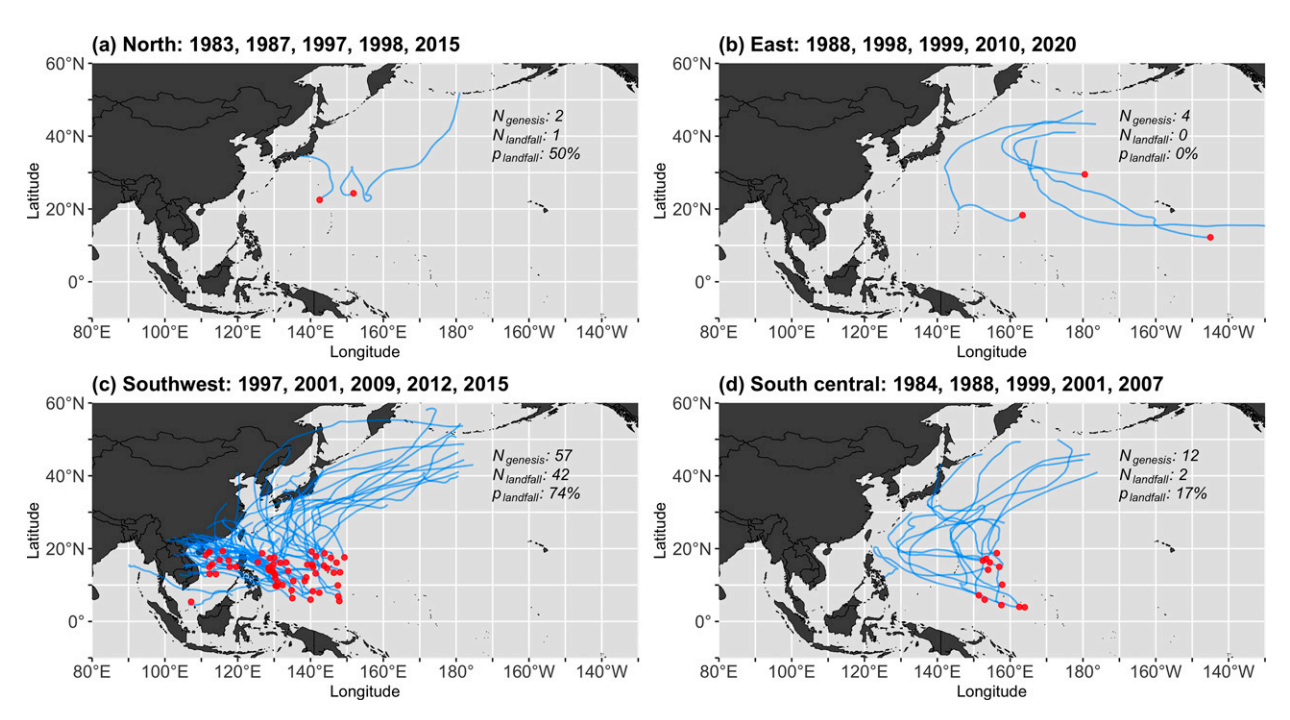


FIG. 9. As in Fig. 8, but for seasons that have Niño-3.4 and WPSH indices located in low modeled landfall count (dark colors) in Fig. 6 for each region.

WNP basin, the seasonal landfall count increases sharply during an El Niño and a strong WPSH. In the east WNP basin, seasonal landfall count increases during an El Niño and a weak WPSH. Last, in the north WNP basin, seasonal landfall count increases during a La Niña and a weak WPSH.

One novel aspect of this study is decomposing TC activity spatially into $10^{\circ} \times 10^{\circ}$ bins to identify distinct regions where genesis and landfall probability are sensitive to environmental conditions through the product of a Poisson and logistic model. Through trial and error, $10^{\circ} \times 10^{\circ}$ bins provide the highest resolution to capture the distinct east-west dipole in TC genesis and the north-south dipole in landfall probability given the limited data. Although we use the Niño-3.4 and WPSH indices, this framework was designed to be flexible, such that it could incorporate additional parameters that are sensitive to genesis and landfall probability. For instance, our study does not differentiate between ENSO flavors such as eastern or central-type events, nor the Pacific meridional mode (PMM) and the Pacific decadal oscillation (PDO) (Chan 2008; Zhang et al. 2012; Capotondi et al. 2015). Nor does this study consider other atmospheric parameters that may have a dependence on TC genesis or landfall probability, such as the tropical intraseasonal oscillation (ISO), the Madden-Julian oscillation (MJO), or the North Atlantic Oscillation (NAO) (Chan 1995; Madden and Julian 1972; B. Wang et al. 2013; Chen et al. 2019; Liu et al. 2021; Nakano et al. 2021). Instead, to introduce this statistical framework as simply as possible, we focused on two low-frequency parameters that modulate landfalls on monthly-to-seasonal time scales. Furthermore, we simply define landfall as "yes" or

"no": in other words, the framework could easily be adopted and modified to focus on landfall in a specific region such as the Southeast Asia coast or the Japan coast instead of the entire Asia coastline. In this study, our goal was not to predict TC landfalls but rather to introduce a new framework elucidating the environmental controls on seasonal landfall by considering TC genesis and landfall separately. The notion that high SSTs associated with ENSO support more TCs and stronger steering flow associated with a WPSH promotes more landfalls are physically intuitive. Our model framework serves to quantify these dependencies on genesis and landfall.

Our statistical framework may be applied to other ocean basins, such as the Indian Ocean, the South Pacific, or the North Atlantic (Ramsay 2017). For instance, in the Atlantic basin, Hart et al. (2016) show a similar spatial pattern of landfall probability as found here in the WNP and suggest variability in landfall count is attributed to ENSO. Whereas in our statistical framework, we consider ENSO primarily as a thermodynamic variable for WNP genesis, another variable such as the Atlantic multidecadal oscillation (AMO) may be a better thermodynamic predictor to assess dependencies on seasonal Atlantic landfalls. Other studies show similar models to assess physical mechanisms and estimate TC genesis and landfalls in the north Indian Ocean through Poisson regressions and generalized additive models (Wahiduzzaman et al. 2021; Wahiduzzaman and Yeasmin 2019). Another study decomposed TC tracks into basinwide TC frequency, spatial genesis distribution, and preferable tracks, showing a relationship between decadal components of ENSO and steering flow related to TC tracks (Yokoi and Takayabu 2013). Compared

to previous studies, we attempt to estimate regional, seasonal TC landfall count based on the dependencies of certain environmental parameters.

While we treat ENSO and the WPSH as independent in our statistical framework due to the weak summer and early fall relationship, studies show that these two variables may covary through ocean–atmosphere interactions (Xie et al. 2016). In contrast to our study, B. Wang et al. (2013) found a significant relationship between the WPSH and WNP basin TC genesis through a principal component (PC) analysis of the WPSH. They decomposed the JJA WPSH into two modes, accounting for 74% of WPSH variability: PC1 related to the zonal dipole of SST anomalies in the Indo-Pacific region and PC2 related to ENSO. Applying a similar method for the JJA period, we also capture a similar east-west dipole in TC genesis, but decomposing the WPSH into two modes obscures the north-south dipole in TC landfall probability found in this study (not shown). A limitation of our simple framework is it cannot differentiate between modes of the WPSH if this framework is applied utilizing ENSO and WPSH predictions from a dynamical model. Another proposed mechanism for the WPSH suggests that post-ENSO summers can exert a significant impact on the WPSH through changes in SST anomalies in the Indian Ocean, which induces a Matsuno (1966)–Gill (1980) response that impacts the WPSH (Xie et al. 2016). In addition to Indian-tropical Pacific interbasin ocean interactions, a source of WPSH and ENSO variability may originate from the tropical Atlantic Ocean or the North Atlantic Oscillation (B. Wang et al. 2013; Johnson et al. 2020; Chikamoto et al. 2020). Some studies further suggest TCs may play an active role in ENSO dynamics. Because TCs are more common in El Niño years, they may contribute to westerly wind bursts and potentially amplify El Niño events through Bjerknes feedbacks (Keen 1982; Harrison and Giese 1991; Kindle and Phoebus 1995; Sobel and Camargo 2005). These studies suggest a complex relationship between ENSO, the WPSH, and WNP TC activity, warranting continued research.

Acknowledgments. Z. F. Johnson and D. R. Chavas were supported by National Science Foundation AGS 1945113. H. A. Ramsay acknowledges support from the Climate Systems Hub of the Australian Government's National Environmental Science Program (NESP). Two anonymous reviewers provided helpful comments that improved the quality of this manuscript.

Data availability statement. All data used in this study can be obtained free of charge to any member of the public. COBE-SST can be obtained from NOAA/OAR/ESRL PSD, Boulder, Colorado, (https://psl.noaa.gov/data/gridded). ERA5 data can be obtained from ECMWF Copernicus (https://cds.climate.copernicus.eu). IBTrACS version 4 can be obtained from NOAA/National Centers for Environmental Information (https://www.ncdc.noaa.gov/ibtracs). All analyses and plotting were performed using the NCAR command language (NCL) and R. The code used in this study can be requested from the corresponding author.

REFERENCES

- Camargo, S. J., and A. H. Sobel, 2005: Western North Pacific tropical cyclone intensity and ENSO. J. Climate, 18, 2996– 3006, https://doi.org/10.1175/JCLI3457.1.
- —, K. A. Emanuel, and A. H. Sobel, 2007: Use of a genesis potential index to diagnose ENSO effects on tropical cyclone genesis. *J. Climate*, 20, 4819–4834, https://doi.org/10.1175/JCLI4282.1.
- Camp, J., M. Roberts, C. MacLachlan, E. Wallace, L. Hermanson, A. Brookshaw, A. Arribas, and A. A. Scaife, 2015: Seasonal forecasting of tropical storms using the Met Office GloSea5 seasonal forecast system. *Quart. J. Roy. Meteor. Soc.*, 141, 2206–2219, https://doi.org/10.1002/qj.2516.
- —, and Coauthors, 2019: The western Pacific subtropical high and tropical cyclone landfall: Seasonal forecasts using the Met Office GloSea5 system. *Quart. J. Roy. Meteor. Soc.*, **145**, 105–116, https://doi.org/10.1002/qj.3407.
- Capotondi, A., and Coauthors, 2015: Understanding ENSO diversity. Bull. Amer. Meteor. Soc., 96, 921–938, https://doi.org/10.1175/BAMS-D-13-00117.1.
- Chan, J. C. L., 1985: Tropical cyclone activity in the Northwest Pacific in relation to the El Niño/Southern Oscillation phenomenon. *Mon. Wea. Rev.*, 113, 599–606, https://doi.org/10. 1175/1520-0493(1985)113<0599:TCAITN>2.0.CO;2.
- —, 1995: Tropical cyclone activity in the western North Pacific in relation to the stratospheric quasi-biennial oscillation. *Mon. Wea. Rev.*, 123, 2567–2571, https://doi.org/10.1175/1520-0493(1995)123<2567:TCAITW>2.0.CO;2.
- —, 2008: Decadal variations of intense typhoon occurrence in the western North Pacific. *Proc. Roy. Soc.*, **464A**, 249–272, https://doi.org/10.1098/rspa.2007.0183.
- Chen, J.-M., C.-H. Wu, J. Gao, P.-H. Chung, and C.-H. Sui, 2019: Migratory tropical cyclones in the South China Sea modulated by intraseasonal oscillations and climatological circulations. J. Climate, 32, 6445–6466, https://doi.org/10. 1175/JCLI-D-18-0824.1.
- ——, P.-H. Lin, C.-H. Wu, and C.-H. Sui, 2020: Track variability of South China Sea–formed tropical cyclones modulated by seasonal and intraseasonal circulations. *Terr. Atmos. Oceanic* Sci., 31, 239–259, https://doi.org/10.3319/TAO.2019.11.07.02.
- Chen, P., M. P. Hoerling, and R. M. Dole, 2001: The origin of the subtropical anticyclones. *J. Atmos. Sci.*, **58**, 1827–1835, https:// doi.org/10.1175/1520-0469(2001)058<1827:TOOTSA>2.0. CO:2.
- Chen, T.-C., S.-Y. Wang, M.-C. Yen, and A. J. Clark, 2009: Impact of the intraseasonal variability of the western North Pacific large-scale circulation on tropical cyclone tracks. Wea. Forecasting, 24, 646–666, https://doi.org/10. 1175/2008WAF2222186.1.
- Chia, H. H., and C. F. Ropelewski, 2002: The interannual variability in the genesis location of tropical cyclones in the northwest Pacific. *J. Climate*, 15, 2934–2944, https://doi.org/10.1175/1520-0442(2002)015<2934:TIVITG>2.0.CO;2.
- Chikamoto, Y., Z. F. Johnson, S.-Y. S. Wang, M. J. McPhaden, and T. Mochizuki, 2020: El Niño–Southern Oscillation evolution modulated by Atlantic forcing. *J. Geophys. Res. Oceans*, 125, e2020JC016318, https://doi.org/10.1029/2020JC016318.
- Choi, W., C.-H. Ho, C.-S. Jin, J. Kim, S. Feng, D.-S. R. Park, and J.-K. E. Schemm, 2016: Seasonal forecasting of intense tropical cyclones over the North Atlantic and the western North Pacific basins. *Climate Dyn.*, 47, 3063–3075, https://doi.org/10. 1007/s00382-016-3013-y.

- Christensen, R., 2006: Log-Linear Models and Logistic Regression. Springer Science & Business Media, 484 pp.
- Clark, J., and P.-S. Chu, 2002: Interannual variation of tropical cyclone activity over the central North Pacific. J. Meteor. Soc. Japan, 80, 403–418, https://doi.org/10.2151/jmsj.80.403.
- Dong, K., 1988: El Niño and tropical cyclone frequency in the Australian region and the northwest Pacific. Aust. Meteor. Mag., 36, 219–225.
- Elsner, J. B., and K.-B. Liu, 2003: Examining the ENSO-typhoon hypothesis. *Climate Res.*, **25**, 43–54, https://doi.org/10.3354/cr025043.
- —, and C. P. Schmertmann, 1993: Improving extended-range seasonal predictions of intense Atlantic hurricane activity. Wea. Forecasting, 8, 345–351, https://doi.org/10.1175/1520-0434(1993)008<0345:IERSPO>2.0.CO;2.
- George, J. E., and W. M. Gray, 1977: Tropical cyclone recurvature and nonrecurvature as related to surrounding wind-height fields. *J. Appl. Meteor.*, **16**, 34–42, https://doi.org/10.1175/1520-0450(1977)016<0034:TCRANA>2.0.CO;2.
- Gill, A. E., 1980: Some simple solutions for heat-induced tropical circulation. *Quart. J. Roy. Meteor. Soc.*, **106**, 447–462, https://doi.org/10.1002/qj.49710644905.
- Gray, W. M., 1979: Hurricanes: Their formation, structure and likely role in the tropical circulation. *Meteorology over the Tropical Oceans*, D. B. Shaw, Ed., Royal Meteorological Society, 155–218.
- —, and J. Sheaffer, 1991: El Niño and QBO influences on tropical cyclone activity. *Teleconnections Linking Worldwide: Anomalies Scientific Basis and Societal Impact*, M. H. Glantz, R. W. Katz, and N. Nicholls, Eds., Cambridge University Press, 257–284.
- Ham, Y.-G., J.-S. Kug, J.-Y. Park, and F.-F. Jin, 2013: Sea surface temperature in the North tropical Atlantic as a trigger for El Niño/Southern Oscillation events. *Nat. Geosci.*, 6, 112–116, https://doi.org/10.1038/ngeo1686.
- Harrison, D. E., and B. S. Giese, 1991: Episodes of surface westerly winds as observed from islands in the western tropical Pacific. J. Geophys. Res., 96, 3221–3237, https://doi.org/10.1029/90JC01775.
- Hart, R. E., D. R. Chavas, and M. P. Guishard, 2016: The arbitrary definition of the current Atlantic major hurricane landfall drought. *Bull. Amer. Meteor. Soc.*, 97, 713–722, https://doi.org/10.1175/BAMS-D-15-00185.1.
- Hersbach, H., 2016: The ERA5 atmospheric reanalysis. 2016 Fall Meeting, San Francisco, CA, Amer. Geophys. Union, Abstract NG33D-01.
- Hoskins, B., 1996: On the existence and strength of the summer subtropical anticyclones: Bernhard Haurwitz memorial lecture. *Bull. Amer. Meteor. Soc.*, 77, 1287–1292.
- Ishii, M., A. Shouji, S. Sugimoto, and T. Matsumoto, 2005: Objective analyses of sea-surface temperature and marine meteorological variables for the 20th century using ICOADS and the Kobe collection. *Int. J. Climatol.*, 25, 865–879, https://doi.org/10.1002/joc.1169.
- Johnson, Z. F., Y. Chikamoto, S.-Y. S. Wang, M. J. McPhaden, and T. Mochizuki, 2020: Pacific decadal oscillation remotely forced by the equatorial Pacific and the Atlantic Oceans. *Climate Dyn.*, 55, 789–811, https://doi.org/10.1007/s00382-020-05295-2.
- Keen, R. A., 1982: The role of cross-equatorial tropical cyclone pairs in the Southern Oscillation. Mon. Wea. Rev., 110, 1405–1416, https://doi.org/10.1175/1520-0493(1982)110<1405: TROCET>2.0.CO;2.

- Kim, H.-M., P. J. Webster, and J. A. Curry, 2011: Modulation of North Pacific tropical cyclone activity by three phases of ENSO. J. Climate, 24, 1839–1849, https://doi.org/10.1175/ 2010JCLI3939.1.
- Kim, J.-H., C.-H. Ho, and P.-S. Chu, 2010: Dipolar redistribution of summertime tropical cyclone genesis between the Philippine Sea and the northern South China Sea and its possible mechanisms. J. Geophys. Res., 115, D06104, https://doi.org/10. 1029/2009JD012196.
- Kindle, J. C., and P. A. Phoebus, 1995: The ocean response to operational westerly wind bursts during the 1991–1992 El Niño. J. Geophys. Res., 100, 4893–4920, https://doi.org/10.1029/94JC02392.
- Knapp, K. R., M. C. Kruk, D. H. Levinson, H. J. Diamond, and C. J. Neumann, 2010: The International Best track Archive for Climate Stewardship (IBTrACS) unifying tropical cyclone data. *Bull. Amer. Meteor. Soc.*, 91, 363–376, https://doi.org/10. 1175/2009BAMS2755.1.
- Lander, M. A., 1994: An exploratory analysis of the relationship between tropical storm formation in the western North Pacific and ENSO. *Mon. Wea. Rev.*, **122**, 636–651, https://doi.org/10.1175/1520-0493(1994)122<0636:AEAOTR>2.0.CO;2.
- Liu, C., W. Zhang, F. Jiang, M. F. Stuecker, and Z. Huang, 2021: Record-low WNP tropical cyclone activity in early summer 2020 due to Indian Ocean warming and Madden-Julian Oscillation activity. *Geophys. Res. Lett.*, 48, e2021GL094578, https://doi.org/10.1029/2021GL094578.
- Lu, M.-M., P.-S. Chu, and Y.-C. Lin, 2010: Seasonal prediction of tropical cyclone activity near Taiwan using the Bayesian multivariate regression method. *Wea. Forecasting*, 25, 1780–1795, https://doi.org/10.1175/2010WAF2222408.1.
- Madden, R. A., and P. R. Julian, 1972: Description of global-scale circulation cells in the tropics with a 40–50 day period. *J. Atmos. Sci.*, **29**, 1109–1123, https://doi.org/10.1175/1520-0469(1972)029<1109:DOGSCC>2.0.CO;2.
- Matsuno, T., 1966: Quasi-geostrophic motions in the equatorial area. J. Meteor. Soc. Japan, 44, 25–43, https://doi.org/10.2151/ jmsj1965.44.1_25.
- Mei, W., and S.-P. Xie, 2016: Intensification of landfalling typhoons over the northwest Pacific since the late 1970s. *Nat. Geosci.*, **9**, 753–757, https://doi.org/10.1038/ngeo2792.
- Miyasaka, T., and H. Nakamura, 2005: Structure and formation mechanisms of the Northern Hemisphere summertime subtropical highs. J. Climate, 18, 5046–5065, https://doi.org/10. 1175/JCL13599.1.
- Nakano, M., F. Vitart, and K. Kikuchi, 2021: Impact of the boreal summer intraseasonal oscillation on typhoon tracks in the western North Pacific and the prediction skill of the ECMWF model. *Geophys. Res. Lett.*, 48, e2020GL091505, https://doi. org/10.1029/2020GL091505.
- Ramsay, H., 2017: The Global Climatology of Tropical Cyclones. Oxford University Press, https://doi.org/10.1093/acrefore/ 9780199389407.013.79.
- Saunders, M. A., R. E. Chandler, C. J. Merchant, and F. P. Roberts, 2000: Atlantic hurricanes and NW Pacific typhoons: ENSO spatial impacts on occurrence and landfall. *Geophys. Res. Lett.*, 27, 1147–1150, https://doi.org/10.1029/1999GL010948.
- Seager, R., R. Murtugudde, N. Naik, A. Clement, N. Gordon, and J. Miller, 2003: Air–sea interaction and the seasonal cycle of the subtropical anticyclones. J. Climate, 16, 1948–1966, https:// doi.org/10.1175/1520-0442(2003)016<1948:AIATSC>2.0.CO;2.

- Sobel, A. H., and S. J. Camargo, 2005: Influence of western North Pacific tropical cyclones on their large-scale environment. J. Atmos. Sci., 62, 3396–3407, https://doi.org/10.1175/JAS3539.1.
- Sun, C., Y. Liu, J. Xue, F. Kucharski, J. Li, and X. Li, 2021: The importance of inter-basin atmospheric teleconnection in the SST footprint of Atlantic Multidecadal Oscillation over western Pacific. *Climate Dyn.*, 57, 239–252, https://doi.org/10.1007/ s00382-021-05705-z.
- Ting, M., 1994: Maintenance of northern summer stationary waves in a GCM. *J. Atmos. Sci.*, **51**, 3286–3308, https://doi.org/10. 1175/1520-0469(1994)051<3286:MONSSW>2.0.CO;2.
- Vecchi, G. A., and G. Villarini, 2014: Next season's hurricanes. Science, 343, 618–619, https://doi.org/10.1126/science.1247759.
- Wahiduzzaman, M., and A. Yeasmin, 2019: Statistical forecasting of tropical cyclone landfall activities over the North Indian Ocean rim countries. *Atmos. Res.*, 227, 89–100, https://doi. org/10.1016/j.atmosres.2019.04.034.
- —, K. Cheung, J.-J. Luo, P. K. Bhaskaran, S. Tang, and C. Yuan, 2021: Impact assessment of Indian Ocean dipole on the North Indian Ocean tropical cyclone prediction using a statistical model. *Climate Dyn.*, 58, 1275–1292, https://doi.org/10.1007/s00382-021-05960-0.
- Wang, B., and J. C. L. Chan, 2002: How strong ENSO events affect tropical storm activity over the western North Pacific. *J. Climate*, **15**, 1643–1658, https://doi.org/10.1175/1520-0442(2002)015<1643:HSEEAT>2.0.CO;2.
- —, B. Xiang, and J.-Y. Lee, 2013: Subtropical high predictability establishes a promising way for monsoon and tropical storm predictions. *Proc. Natl. Acad. Sci. USA*, **110**, 2718–2722, https://doi.org/10.1073/pnas.1214626110.
- Wang, C., and B. Wang, 2019: Tropical cyclone predictability shaped by western Pacific subtropical high: Integration of trans-basin sea surface temperature effects. *Climate Dyn.*, 53, 2697–2714, https://doi.org/10.1007/s00382-019-04651-1.
- —, and L. Wu, 2016: Interannual shift of the tropical uppertropospheric trough and its influence on tropical cyclone formation over the western North Pacific. J. Climate, 29, 4203–4211, https://doi.org/10.1175/JCLI-D-15-0653.1.
- —, C. Li, M. Mu, and W. Duan, 2013: Seasonal modulations of different impacts of two types of ENSO events on tropical cyclone activity in the western North Pacific. *Climate Dyn.*, 40, 2887–2902, https://doi.org/10.1007/s00382-012-1434-9.
- ——, B. Wang, and L. Wu, 2019: A region-dependent seasonal forecasting framework for tropical cyclone genesis frequency in the western North Pacific. *J. Climate*, 32, 8415–8435, https://doi.org/10.1175/JCLI-D-19-0006.1.
- Wang, S., and R. Toumi, 2021: Recent migration of tropical cyclones toward coasts. *Science*, 371, 514–517, https://doi.org/10.1126/science.abb9038.
- —, and —, 2022: On the intensity decay of tropical cyclones before landfall. Sci. Rep., 12, 3288, https://doi.org/10.1038/ s41598-022-07310-4.
- Williams, I. N., and C. M. Patricola, 2018: Diversity of ENSO events unified by convective threshold sea surface temperature: A nonlinear ENSO index. *Geophys. Res. Lett.*, 45, 9236–9244, https://doi.org/10.1029/2018GL079203.
- Wu, G., and N.-C. Lau, 1992: A GCM simulation of the relationship between tropical-storm formation and ENSO. Mon. Wea. Rev., 120, 958–977, https://doi.org/10.1175/1520-0493(1992) 120<0958:AGSOTR>2.0.CO;2.

- —, and Y. Liu, 2003: Summertime quadruplet heating pattern in the subtropics and the associated atmospheric circulation. *Geophys. Res. Lett.*, 30, 1201, https://doi.org/10.1029/ 2002GL016209.
- Wu, L., and B. Wang, 2004: Assessing impacts of global warming on tropical cyclone tracks. J. Climate, 17, 1686–1698, https://doi. org/10.1175/1520-0442(2004)017<1686:AIOGWO>2.0.CO;2.
- Wu, M. C., W. L. Chang, and W. M. Leung, 2004: Impacts of El Niño–Southern Oscillation events on tropical cyclone landfalling activity in the western North Pacific. *J. Climate*, 17, 1419–1428, https://doi.org/10.1175/1520-0442(2004)017<1419: IOENOE>2.0.CO:2.
- Xiang, B., B. Wang, W. Yu, and S. Xu, 2013: How can anomalous western North Pacific subtropical high intensify in late summer? *Geophys. Res. Lett.*, 40, 2349–2354, https://doi.org/10. 1002/grl.50431.
- Xie, S.-P., Y. Kosaka, Y. Du, K. Hu, J. S. Chowdary, and G. Huang, 2016: Indo-western Pacific Ocean capacitor and coherent climate anomalies in post-ENSO summer: A review. Adv. Atmos. Sci., 33, 411–432, https://doi.org/10.1007/s00376-015-5192-6.
- Yang, J., and M. Chen, 2021: Variations of rapidly intensifying tropical cyclones and their landfalls in the western North Pacific. Coastal Eng. J., 63, 142–159, https://doi.org/10. 1080/21664250.2021.1909966.
- Yokoi, S., and Y. N. Takayabu, 2013: Attribution of decadal variability in tropical cyclone passage frequency over the western North Pacific: A new approach emphasizing the genesis location of cyclones. *J. Climate*, 26, 973–987, https://doi.org/10.1175/JCLI-D-12-00060.1.
- Yonekura, E., and T. M. Hall, 2011: A statistical model of tropical cyclone tracks in the western North Pacific with ENSOdependent cyclogenesis. *J. Appl. Meteor. Climatol.*, 50, 1725– 1739, https://doi.org/10.1175/2011JAMC2617.1.
- Zhang, W., H.-F. Graf, Y. Leung, and M. Herzog, 2012: Different El Niño types and tropical cyclone landfall in East Asia. *J. Climate*, 25, 6510–6523, https://doi.org/10.1175/JCLI-D-11-00488.1.
- —, G. A. Vecchi, G. Villarini, H. Murakami, R. Gudgel, and X. Yang, 2017: Statistical–dynamical seasonal forecast of western North Pacific and East Asia landfalling tropical cyclones using the GFDL FLOR coupled climate model. *J. Climate*, 30, 2209–2232, https://doi.org/10.1175/JCLI-D-16-0487.1.
- Zhao, H., and L. Wu, 2014: Inter-decadal shift of the prevailing tropical cyclone tracks over the western North Pacific and its mechanism study. *Meteor. Atmos. Phys.*, 125, 89–101, https:// doi.org/10.1007/s00703-014-0322-8.
- —, and C. Wang, 2019: On the relationship between ENSO and tropical cyclones in the western North Pacific during the boreal summer. *Climate Dyn.*, **52**, 275–288, https://doi.org/10.1007/s00382-018-4136-0.
- —, L. Wu, and W. Zhou, 2010: Assessing the influence of the ENSO on tropical cyclone prevailing tracks in the western North Pacific. Adv. Atmos. Sci., 27, 1361–1371, https://doi.org/ 10.1007/s00376-010-9161-9.
- Zhou, X., and R. Lu, 2019: Interannual variability of the tropical cyclone landfall frequency over the southern and northern regions of East Asia in autumn. *J. Climate*, **32**, 8677–8686, https://doi.org/10.1175/JCLI-D-19-0057.1.